Theoretical Modeling of a Copper Site in a Cu(II)−Y Zeolite

Dorothée Berthomieu,* Saïlaja Krishnamurty, Bernard Coq, Gérard Delahay, and Annick Goursot

Laboratoire de Matériaux Catalytiques et Catalyse en Chimie Organique, UMR CNRS−5618, ENSCM, 8, rue de l'Ecole Normale, 34296 MONTPELLIER Cédex 5, France

Received: August 10, 2000; In Final Form: November 27, 2000

Model clusters of a Cu(II)−Y zeolite have been studied using a density functional theory based method in order to investigate the electronic properties of the metal site involved in the catalytic activity of this zeolite. This work has shown that different Si/Al ratios, sizes, and shapes of the models do not induce significant changes in the electronic properties of the Cu site, whereas the influence of its coordination is emphasized. A large charge transfer (CT) from the zeolite to the metal has been found in the case of a formal Cu(II) cation. Comparable net charges on Cu are thus obtained for models of Cu(II) and Cu(I)-zeolite. However, these two systems differ by their frontier orbital patterns, which are characterized by a low lying empty orbital localized on the zeolite and on Cu in the case of Cu (II), whereas the lowest virtual molecular orbital of the Cu(I) model has a much higher energy. Addition of NH_3 molecules to the Cu(II) model is accompanied by a rearrangement in the electron distribution of the whole system, underlying the non negligible role of the zeolite in the catalytic process.

I. Introduction

The selective catalytic reduction (SCR) by various reductants is the best controlled technology for NO_x removal from both stationary and mobile sources. Cu-exchanged zeolites are among the most efficient materials in SCR by NH_3 from stationary sources, and they exhibit a widely open temperature operation range.[1−3] The relevance of Cu(II)/Cu(I) redox cycle was demonstrated, as was the requirement of O_2 to boost the SCR rate. On copper-exchanged faujasite, it was proposed that Cu^{2+} is reduced by NO + NH_3 to Cu^+, which in turn is oxidized to Cu^{2+} by NO + O_2, faster than by O_2 alone.[4] The most active sites are formed by Cu ions stabilized by NH_3 and located in the supercage of the faujasite. Different intermediates have been proposed, but no molecular proof of the mechanism has been established. It is thus worthwhile to study the proposed reaction paths in order to make progress in the knowledge of the catalytic behavior of such transition metal cation-exchanged zeolites in order to further design optimized materials.

Few works are devoted to the theoretical study of the transformation of NO_x in Cu-exchanged zeolites, and only very few are concerned with Cu(II) cations.[5−9] Our interest is to study, in a first step, the electronic properties of a Cu(II) site of faujasite in order to understand its reactivity and also to model how it bonds to NH_3, which is acting as a reductant in the catalytic process. The first requirement to such a study is to find a valuable representation for the active site. Different methods have been used to model active sites such as force fields, cluster models, embedding techniques, periodic calculations.[10−13] Comparing the active site with a metal complex, we have chosen to represent the local part of the solid involved in the active site and to study it using a quantum mechanical method. Previous theoretical calculation results on ZSM5 models showed that the use of a low coordination environment for Cu and isoelectronic atoms instead of the real ones did not yield accurate binding energies.[5,9] Moreover, this modeling would be inadequate for the description of a catalytic cycle, failing to describe the electronic properties of the metal center. Clusters of different sizes and shapes have been compared in order to evaluate the influence of the model on the electronic properties of Cu(II).

Negative charges borne by the zeolite framework are compensated by protons, alkali and/or transition metal cations for instance. A proton makes a covalent bond with one oxygen atom, whereas alkaline cations keep essentially their positive charge with small calculated charge transfers (CT) from the zeolite to the cations (smaller than 0.1 for monocharged cations and less than 0.2−0.3 for doubly charge cations such as Ca^{2+}).[13] Alkaline cations have closed p^6 shells and their electron affinity is small. Transition metal cations in zeolites should react differently from alkalis, and the framework anion is expected to transfer some electronic charge to empty d orbitals.

The second ionization energy of copper is the largest in the first row of transition metals (20.3 eV), indicating that the electron affinity of Cu(II) is very substantial. The energy difference with ligand ionization energies is expected to lead to an important electron donation from the ligands to the transition metal. Actually, it is usually very difficult to generate Cu(II) complexes in gas phase, and no binding energies have been determined experimentally.[14,15] In a previous study by Schneider et al.[16] of a model of Cu(II) in ZSM5, the charge calculated on the formal Cu(II) ion was very close to +1. Although these authors did not comment on this value, we think that it can be attributed to a CT effect, which achieves a very stable d^{10} configuration. Because a copper cation interacting with a zeolite framework should differ from an isolated cation for reactions with other ligands such as NH_3, we have found it advisable to study first Cu(II) sites in a Cu−Y zeolite before studying their behavior in the presence of incoming molecules. This is the aim of the present detailed analysis of a Cu(II) site using various models for the local representation of the zeolite

* Corresponding author. E-mail bertho@crit1.univ-montp2.fr

10.1021/jp002929b CCC: $20.00
Published on Web 01/12/2001

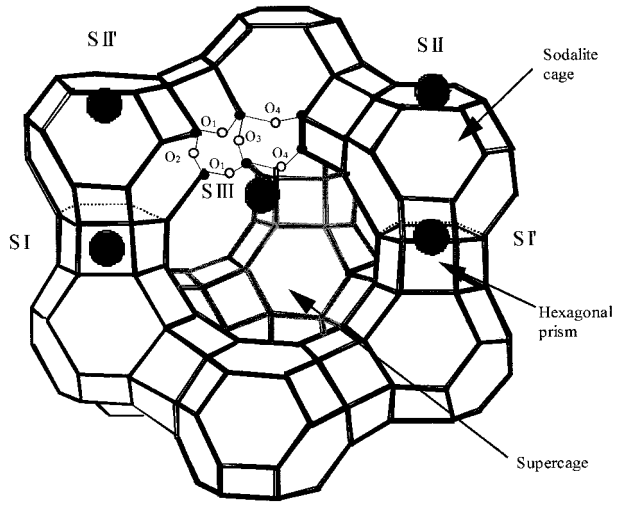

Figure 1. Faujasite type structure with cationic sites. Cu in site III position is bicoordinated to O_1 and O_4.

and analyzing the effect of the choice of this model on the electronic structure of copper. This analysis is presented in the first part of the results (III.1). The second part (III.2) is devoted to the investigation of NH_3 complexation with the active site.

II. Methodology

1. Models. Faujasite-type zeolites have a three-dimensional framework built of tetrahedral SiO_4 and AlO_4 units linked together to form four- and six-membered rings connected into hexagonal prisms and sodalite cages. Their formation creates subsequently large cavities called supercages. One negative charge is induced in the framework whenever a Si center is replaced by Al. The Al/Si ratio is controlled during the synthesis, although Al positions are not known. Y zeolites are faujasite-type zeolites with a Si/Al ratio of 2:3. The negative charges are compensated by exchangeable cations that may be protons, alkaline, or transition metal cations.

The cations exchanged in a Y-zeolite may occupy different crystallographic sites (Figure 1). Conventionally, O atoms are labeled with respect to the ring types in which they are involved (Figure 1). According to X-ray data for a dehydrated Cu−Y zeolite with a Si/Al ratio of 2.42, this corresponds to about 4 site III cations, 7 site II, II′ cations, and 17 site I, I′ cations per unit cell.[17] The interaction energy of cations with the zeolite framework depends on their positions. Whereas it is probably not the most stable cation position, in a dehydrated framework, it has been proposed from experiments that the most active copper species are located at sites III in the supercages.[18] Furthermore, site III Cu(II) cations are most probably bicoordinated to the O_1 and O_4 atoms of the framework (Figure 1).[17]

Interestingly, experiments have shown that it is possible by exchange with Ba^{2+} cations to occupy preferentially sodalite cages and hexagonal prisms and then to further exchange selectively the supercage positions with copper.[4] On the CuBa−Y catalyst, the turn over frequency per Cu atom is much higher than on Cu−Y, which provides evidence that site III cations are the most active sites. We have thus chosen to model the Cu sites together with clusters involving those sites.

To compensate the formal Cu^{2+} charge, two aluminum atoms have always been included in the models. Obeying the Löwenstein rule, they are separated by at least one Si center. Such models must provide a better description of the electronic properties of copper than a system containing silicon atoms and additional negative point charges.[5,9] All models have been terminated with H atoms, the O−H bonds being set to 1.0 Å and the Si−H bonds to 1.5 Å. In order to preserve the original structure of the zeolite, the H atoms have been positioned along the corresponding Si−O bonds of the experimental zeolite Y structure. The models CuY_A, CuY_B, CuY_C, CuY_D reported in Figure 2 correspond to copper located at the X-ray positions.[17] In the models iCuY$_B$ and jCuY$_B$ (Figure 2), Cu−O bond distances have been optimized yielding shorter bonds with the neighboring O atoms in comparison with the four other models. As shown in Figure 1, "ideal" sites, i.e., on top of four-

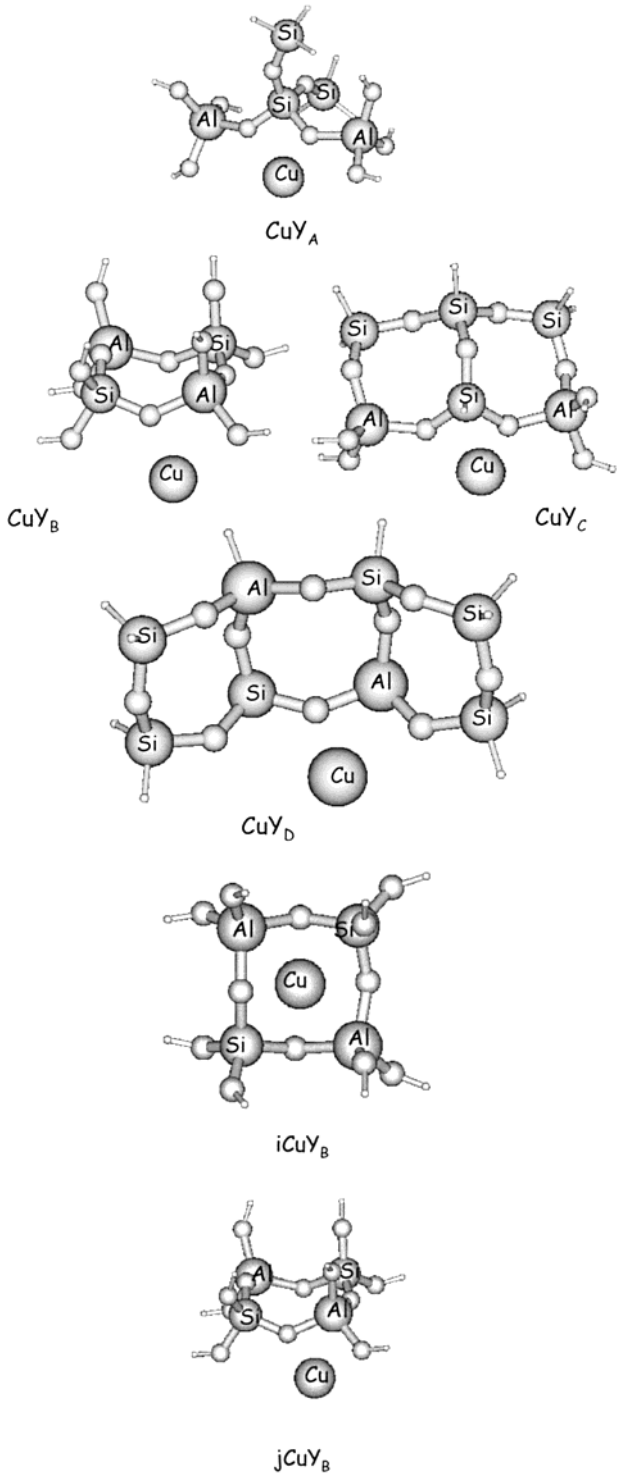

Figure 2. Cluster models CuY_A, CuY_B, CuY_C, CuY_D, iCuY$_B$, and jCuY$_B$ representing the bicoordinated and "ideal" site III.

membered rings, are also available for sites III and have been reported for alkali cations.[19,20] The model *i*CuY_B corresponds to Cu in an ideal position (Figure 2). The CuY_BH model is based on CuY_B, but contains an additional proton bound to ring oxygen, which implies that the copper cation is formally Cu(I).

One must stress that X-ray positions take into account the full zeolite, including the presence of the other cations. A cluster representation gives a partial view, ignoring the cation−cation repulsions that have a significant effect on the cations positions.[21]

2. Calculations. The calculations using density functional theory (DFT) were performed with the deMon[22] or Gaussian programs.[23] Spin unrestricted DFT and unrestricted Hartree−Fock (UHF) methods were used for open-shell systems. All geometry optimizations have been performed using the so-called mixed scheme, i.e., local level of theory for the potential (Vosko−Wilk−Nusair formulation for correlation)[24] and using gradient-corrected (GGA)[25] functionals for the exchange[26] and correlation[27] energies. These calculations are labeled m-BP.

The calculations labeled B3LYP,[28,29] nl-BP, and MP2 [30] have been performed using the Gaussian 98 program and have been carried out using the geometries obtained as previously described.The notation nl-BP indicates that both the potential and the energy are described using GGA functionals, i.e., Becke for exchange[26] and Perdew for correlation.[27]

During geometry optimization, the H atoms terminating the clusters have been kept fixed. In the case of the large cluster CuY_D, only the Cu^{2+} position with respect to the zeolite has been optimized, the zeolite cluster being kept at the experimental geometry.[17]

Geometry optimizations were considered terminated when energy changes were less than 10^{-5} Hartree, corresponding generally to a gradient norm between 0.005 and 0.008. Frequency analysis was not performed for these clusters because geometry optimization with fixed atoms leads to wrong values for normal modes. However, we performed a frequency analysis for the model (H_3NCuY_B), and whereas all of the terminating H atoms of the zeolite were fixed during the geometry optimization, only one very small negative frequency value was calculated, indicating that this structure was related to a minimum and not to a transition state.

Previous works and our own test calculations on small Cu(II) systems have shown that a large basis for Cu is necessary to reproduce metal−ligand binding energies.[31−34] To this end, we have chosen the Wachters basis set (without f orbitals) for copper,[35] whereas all electrons basis sets of DZVP quality have been used for all other heavy atoms and a DZ basis for hydrogen atoms. In Huzinaga's notation their contraction patterns are (6321/521/1*), (621/41/1*), and (41) for Si and Al, O, and H, respectively.[36] The associated auxiliary basis sets used to fit the density and the exchange-correlation potential (deMon code) are, with respect to the same atoms, (5,4;5,4), (5,2;5,2), and (5,1;5,1), where the usual deMon notation is used.[37] The fitting of the exchange-correlation potential has been performed using a grid of 64 radial points and 26 angular points, whereas the energy and its gradient were evaluated using a more extended grid. With the Gaussian 98 code, we have used the Wachters basis set for Cu also and two different all-electron Gaussian basis sets for the others atoms: 6-31G(d) and the triple-ζ quality basis set 6-311+G(2d,2p) for B3LYP and nl-BP calculations. In Huzinaga's notation, the 6-31G(d) contraction patterns are (6631/631/1*) for Si and Al and (631/31/1*) for O; the 6-311+G(2d,2p) corresponding set is (6311111/421111/11*) for Si and Al and (6311/311/11*) for O. MP2 calculations (see III-1-E) have also been performed using a 6-31G(d) basis.

Mulliken and Bader-type[38] population analyses have been used in this study.

The average binding energies of NH_3 to CuY_B (or CuY_BH) have been defined according to the following reaction:

$$H_3N + 1/nCuY_B \rightarrow 1/n[(H_3N)_nCuY_B]$$

with $n = 1$, 2, or 3.

III. Results and Discussion

1. Electronic Properties of Cu(II) Involved in Different Cluster Models. We first studied the influence of the chemical environment on the electronic properties of Cu using the models described in section II. We have compared the electronic properties of Cu involved in these models in order to see the influence of different parameters: shape, size, Al atom distribution, Si/Al ratio, and neighboring environment of Cu. The geometric parameters, the gap between frontier orbitals, the configuration, and the charge of Cu are reported in Table 1. Because all of these models correspond to open-shell systems, the SOMO (singly occupied molecular orbital) occupied by an unpaired electron is the highest occupied orbital. The energy difference between the SOMO and the LUMO (lowest unoccupied molecular orbital) will be considered as the energy gap. The frontier orbitals calculated for these models show a general energy profile with a characteristic low-lying empty LUMO and a mixture of zeolite p O and Cu d orbitals contributing to these SOMO and LUMO.

A. Effect of the Cluster Size. Starting the geometry optimization with a Cu located at the X-ray position (with $Cu-O_1 = 2.2$ and $Cu-O_4 = 2.8$ Å), leads to Cu−O bond lengths closed to the experimental structure, as shown in Table 1 for models CuY_A, CuY_B, CuY_C, and CuY_D. The SOMO−LUMO gap is very small in all cases. The charge and electronic configuration of Cu are also similar for the first three models. The charge on Cu is around +0.8, which is far from a formal +2 value. The Cu 3d participation in the frontier orbitals varies with the models, but these differences are small (between 4 and 23%). Comparison of the properties calculated for the models CuY_B and CuY_D shows that the OH terminations in the four-membered ring system CuY_B lead to results similar to those obtained with OSi terminations in the three four-membered ring system CuY_D: the charge on Cu and its electronic configuration are only slightly changed. The SOMO−LUMO gap is increased in this larger model, but this difference may be explained by the fact that the whole geometry has not been optimized in this cluster. Moreover, comparison of the two clusters CuY_B and CuY_D shows that different Si/Al ratios do not lead to significant changes in the calculated properties.

These results demonstrate that the electronic properties of Cu, i.e., the net charge, electronic configuration and participation in the frontier orbitals are independent of the shape and size of the models considered, as well as of the OH terminations.

B. Effect of the Cu(II) Position in the CuY_B Model. Because different positions are available for sites III, we have found it of interest to look at the influence of the site III position using the models CuY_B, *i*CuY_B, and *j*CuY_B. Cu is in the so-called "ideal" position (connected to two O_1, one O_2, and one O_3) in the model *i*CuY_B, whereas $Cu(II)-O_1$ and $Cu(II)-O_4$ bond lengths are equivalent in the model *j*CuY_B. Optimization of these structures leads to the following order of relative stability: *i*CuY_B (0.0) > *j*CuY_B (26.2) > CuY_B (32.0 kcal/mol). In the *i*CuY_B

TABLE 1: m-BP Structures, SOMO−LUMO Gaps and Types, Mulliken Cu Net Charges, Mulliken Cu 3d, 4s and 4p Populations of the Various Cu(II)-Y Models

model	bond lengths (Å)		OCuO Angles (°)	gap (eV)	SOMO type	LUMO type	Cu Mulliken net charge	Cu configuration
CuY_A	Cu−O	1.85	68.47	0.01	p O,10%d Cu	p O, 17%d Cu	Cu: +0.78	$4s^{0.15}\,4p^{0.17}\,3d^{9.90}$
	Cu−O	2.50						
	(Cu−Si	2.85)						
CuY_B	Cu−O	1.89	72.16	0.09	p O, 23%d Cu	p O, 8% d Cu	Cu: +0.72	$4s^{0.18}\,4p^{0.15}\,3d^{9.95}$
	Cu−O	2.55						
	(Cu−Al	2.92)						
CuY_C	Cu−O	1.86	69.44	0.01	p O, 4%d Cu	p O, 19%d Cu	Cu: +0.79	$4s^{0.15}\,4p^{0.17}\,3d^{9.89}$
	Cu−O	2.45						
	(Cu−Si	2.84)						
CuY_D	Cu−O	1.89	73.14	0.10	p O, 20%d Cu	p O, 7%d Cu	Cu: +0.67	$4s^{0.21}\,4p^{0.16}\,3d^{9.96}$
	Cu−O	2.65						
	(Cu−Al	2.80						
iCuY$_B$	Cu−O	1.99	66.84	0.19	p O, 6% d Cu	p O, 35%d Cu	Cu: +0.82	$4s^{0.13}\,4p^{0.25}\,3d^{9.80}$
	Cu−O	2.02	71.42					
	Cu−O	2.25	72.18					
	Cu−O	2.64	79.06					
	(Cu−Al	2.77)						
	(Cu−Al	2.77)						
jCuY$_B$	Cu−O	1.90	87.96	0.07	p O, 64%d Cu	p O, 15%d Cu	Cu: +0.77	$4s^{0.13}\,4p^{0.19}\,3d^{9.91}$
	Cu−O	1.95						
	(Cu−Al	2.56)						

$Y_A = Si_3Al_2O_{10}H_{12}^{2-}$, $Y_B = Si_2Al_2O_8H_8^{2-}$, $Y_C = Si_4Al_2O_{11}H_9^{2-}$, $Y_D = Si_6Al_2O_8H_{12}^{2-}$

TABLE 2: Relative Energies, m-BP Structures, SOMO−LUMO Gaps, and Mulliken Cu Net Charges of CuY_D

isomer	Cu position	ΔE (kcal/mol)	Bond lengths (Å) Cu−O_1	Cu−O_3	Cu−Al_2	gap (eV)	Cu Mulliken net charge
Al_2/Al_{11}	P1	8.0	2.67	1.89	2.82	0.06	0.61
	P2	0.0	2.10	1.89	2.43	0.10	0.68
	P 3	5.0	1.89	2.65	2.80	0.10	0.67
Al_2/Al_{17}	P′1	16.0	2.68	1.90	2.84	0.06	0.61
	P′2	0.0	1.90	2.01	2.45	0.01	0.65
	P′3	11.7	1.90	2.68	2.84	0.01	0.65
	P′4	21.5	2.19	3.9	3.65	0.01	0.67
	P′5	26.3	2.60	4.7	4.08	0.01	0.68

model, the four-coordination of Cu explains its higher stability compared with the bi-coordinated models CuY_B, jCuY$_B$. Accordingly, the Cu−O bond lengths are also shorter in this model. The energy differences between CuY_B, iCuY$_B$, and jCuY$_B$ have almost no effect on the charge of Cu. However, differences appear in electronic structures: as shown in Table 1, the higher coordination of Cu is related to a larger HOMO−LUMO gap, and because Cu is nearer to O atoms there is an increased metal participation to these orbitals. The analysis of the Cu electronic configuration shows also that a higher coordination (iCuY$_B$) is related to increased 4s and 4p and decreased 3d populations (Table 1).

C. Effect of the Cu(II) Position in the CuY_D Model. The supercage can be represented as an accessible spherical volume with a diameter of ca. 10 Å. CuY_D contains the three-edge, four-membered rings feature, at the edge of the supercage. We have analyzed how the properties of this model change with different Cu and Al positions. Table 2 reports the relative energies for the different Cu positions illustrated in Figure 3. These various positions actually correspond to a shift of Cu along the edge of the four-membered rings. Seven different positions of Cu were investigated with respect to the zeolite framework in which the second Al occupied two different relative positions, *11* and *17* (Figure 3). It comes out that the system is more stable when Cu is near Al rather than Si, as it is expected from experiments, and when the two Cu−O bonds lengths are almost equal. One can also observe that the position of the second Al (from *11* to *17*) does not change the relative energy of the system. These results also show that the electronic configuration and charge of Cu are sensitive neither to the next nearest atoms nor to the cluster size. On this basis, we have considered that we could thus use the simplest system CuY_B for further investigations because the electronic Cu structure does not differ from that of larger models or models with different Al distribution patterns and Si/Al ratios.

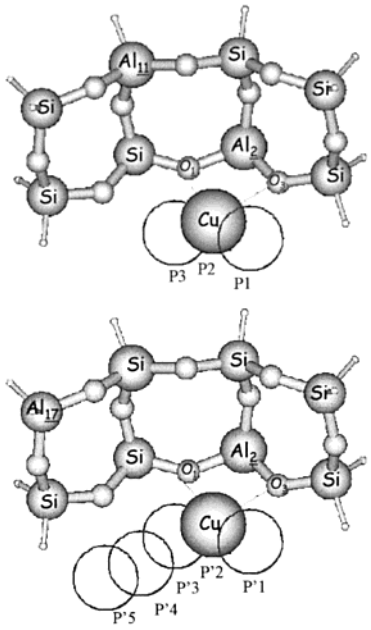

Figure 3. P1, P2, P3 (a) and P′1, P′2, P′3, P′4, P′5 (b) positions of bicoordinated Cu in CuY_D.

TABLE 3: m-BP Structures, Frontier Orbitals Gaps and Types, Mulliken and Bader Metal Net Charges, Mulliken Cu 3d, 4s, and 4p Populations of the Various M−Y_B Complexes

complex	bond lengths (Å) M−O	bond lengths (Å) M-Al	OMO angle (°)	gap (eV)	HOMO type or SOMO type	LUMO type	metal net charge	valence electronic configuration of Cu
NaY_BH	2.04 2.18	2.69	80.10	4.30	p O	s Na	Na: +0.90[a] +0.95[b] H: +0.43[b]	
CuY_BH	1.91 2.63	2.94	71.09	1.68	p O, 81%d Cu	91% s Cu	Cu: +0.71[a] +0.62[b] H: +0.44[b]	$4s^{0.24}\ 4p^{0.16}\ 3d^{9.98}$
$iCaY_B$	2.27 2.28 2.51 2.85	2.99 3.05	60.18 64.28 64.73 70.24	3.29	p O	s Ca	Ca: +1.78[a] +1.34[b]	
CuY_B	1.89 2.55	2.92	72.16	0.09	p O, 23%d Cu	p O, 8%d Cu	Cu: +0.80[a] +0.72[b]	$4s^{0.18}\ 4p^{0.15}\ 3d^{9.95}$

[a] Bader Analysis. [b] Mulliken Analysis.

D. Comparison of Cu(II) with Other Cations. The clear conclusion of the previous sections is that the formal Cu(II) cation bears a much less positive charge (+0.8) than expected regardless of the models used. This behavior has led us to analyze how the CT from the zeolite clusters to the metal is specific to Cu(II). For this purpose, we have chosen the Y_B model associated with the following M cations: (Cu^+, H^+), Ca^{2+}, (Na^+, H^+). Table 3 reports the results obtained for these models involving different metal cations with different oxidation states and coordination types between the metal and the zeolite framework. The changes in the M−O bond lengths follow the variation of the metal ionic radii: they are increasing in the order Cu(II) < Cu(I) < Na(I) < Ca(II).[39] For all systems, the Mulliken and Bader charges are reported: CaY_B is the only model with a significant difference between these two evaluations. Since the charge would be calculated in a more accurate way in the Bader analysis for ionic bonding, the charge on Ca is more likely around +1.8.[38] Except for the formal Cu(II) in CuY_B model, the net metal charges are very close to the expected formal values, showing a very small zeolite-to-metal CT. As one may observe, whatever the coordination of Cu, its charge is very close to that of CuY_BH in which Cu is formally Cu(I). This result is in agreement with experiments that emphasize the great instability of Cu(II):[15,14] the well-known observed CT takes place on contact of ligands with Cu(II) because "the ionization energy of Cu(I) (IE = 20.3 eV) is very high." This CT increases the binding energy of Cu to the zeolite as it is around 3.5 times larger in CuY_B (627 kcal/mol) than in CuY_BH (177 kcal/mol): a simple electrostatic effect would have increased the binding energy by a factor of ca. 2 only. We may notice that this binding energy is very large and should retain the cation at a fixed position, although such estimate does not take into account the electrostatic repulsion with the other cations.[21] As it can be seen from Table 3, a formal Cu(I) in CuY_BH undergoes also a CT from the zeolite, although less important than for Cu(II) but larger than for an alkali. Even if DFT methods are known to overestimate metal−ligand binding and, consequently CT,[40] this behavior is also reproduced by HF-based methods (next section). Moreover, a similar CT trend has also been obtained with other transition metal cations in zeolite models.[41] When the metal involved is Na^+, Ca^{2+}, or a formal Cu(I), the gap between HOMO and LUMO is larger than 1.7 eV, whereas it is very small (less than 0.2 eV) when a formal Cu(II) is involved. In the case of alkaline cations, the p orbitals of zeolite O atoms contribute to the HOMO, whereas the s orbital of the metal participates in the LUMO. The same scheme applies to CuY_BH with an additional contribution of the d orbitals of Cu in the HOMO, whereas these orbitals do not participate in the LUMO. In this case, the HOMO−LUMO gap is smaller than with alkaline cations. CuY_B behaves differently because of a low lying LUMO orbital, and both frontier orbitals correspond to a contribution of O p orbitals and Cu 3d orbitals. The HOMO−LUMO (SOMO−LUMO) energy gap in CuY_B (formal Cu^{2+}) is in fact a gap between two MOs (molecular orbitals) based on combinations of 3d Cu and p O orbitals of comparable energies. In contrast, the gap in CuY_BH (formal Cu^{1+}) corresponds to two MOs of different nature: the HOMO has mainly a 3d Cu character, whereas the LUMO is essentially a 4s Cu orbital (which is the same behavior for alkali). This CuY_B MO profile is characteristic of a Cu(II)-exchanged faujasite and will remain valid after addition of ligands, as we will see further.

E. Influence of the Method on the CuY_B Results. We have found it important to check the validity of our results concerning the ligand-to-metal charge-transfer involving the zeolite anion and the Cu^{2+} cation, by comparing GGA DFT results with B3LYP and MP2 calculations. Whatever the method used, the charge on Cu was found to be less than +1. Increasing the basis on the zeolite atoms, i.e., using a 6-311+G(2d,2p), increases slightly the net positive charge on Cu, which however, remains less than +1. These results indicate that, at this level of theory, a charge transfer occurs from the zeolite to the Cu cation, which reaches a stable d^{10} configuration. The binding energy of Cu to zeolite was calculated to be around 600 kcal/mol using the most extended basis set and B3LYP. The difference between the nl-BP and B3LYP energy values (30 kcal/mol) represents only 5% of this binding energy and is totally compatible with the admixture of HF exchange in the potential based on B3LYP calculation in which the exchange functional is replaced by a linear combination of the Hartree−Fock exchange. Furthermore, no experiments are available that would indicate which method is more accurate.

These results show that a Cu(II)-exchanged faujasite is not characterized by the cationic charge, which is comparable with that of a Cu(I), but more probably by its frontier orbital pattern, i.e., by the presence of a low-lying singly occupied spin−orbital that is delocalized on the metal and the zeolite. This delocalization may be understood as a route the system can follow to receive or donate electrons, the zeolite framework being considered as a reservoir of electronic charge. The so-called oxido−reduction reaction, formally described as a Cu(II)/Cu(I) change accompanied by a proton donation to zeolite, could then be viewed as a rearrangement of the electron distribution in the zeolite with a corresponding change in the orbital pattern. Abstraction of the proton leads to the opposite change, generating the low-lying 3d Cu orbital, described formally as a Cu(I) → Cu(II) back reaction.

TABLE 4: m-BP Structures, Frontier Orbitals Gaps, Mulliken Cu Net Charges and Mulliken Cu 3d, 4s, and 4p Populations and Average N−Cu Binding Energies (kcal/mol) of Cu(I) and Cu(II) Complexes

complex	bond lengths (Å) Cu−O_1	Cu−O_2	Cu−N	OCuO angle (°)	gap (eV)	Cu Mulliken net charge	valence electronic configuration of Cu	average N-Cu binding energy m-BP86 (kcal/mol)
CuY_B	1.89	2.55		72.2	0.09	Cu: +0.72	$4s^{0.18}\,4p^{0.15}\,3d^{9.95}$	
H_3NCu^{1+}			1.84		2.83	Cu: +0.73	$4s^{0.26}\,4p^{0.06}\,3d^{9.95}$	67.2
H_3NCu^{2+}			1.89		0.68	Cu: +1.36	$4s^{0.0}\,4p^{0.03}\,3d^{9.61}$	162.6
$(H_3N)_4Cu^{2+}$ square planar C_{2v}			2.04		0.61	Cu: +0.92	$4s^{0.28}4p^{0.20}\,3d^{9.60}$	96.5(96.9)[a]
$(H_3N)CuY_B$	1.89	2.55	2.02	72.3	0.03	Cu: +0.60	$4s^{0.39}4p^{0.21}\,3d^{9.80}$	49.9
$(H_3N)_2CuY_B$	2.00	2.52	1.98 2.00	73.4	0.06	Cu: +0.74	$4s^{0.30}4p^{0.27}\,3d^{9.69}$	30.8
$(H_3N)_3CuY_B$	1.91	2.52	1.97 2.02 2.02	73.5	0.08	Cu: +0.81	$4s^{0.18}4p^{0.33}\,3d^{9.68}$	19.1
$(H_3N)CuY_BH$	1.89	2.56	1.96	73.4	3.17	Cu: +0.49	$4s^{0.47}4p^{0.20}\,3d^{9.84}$	56.5

[a] Reference [42]

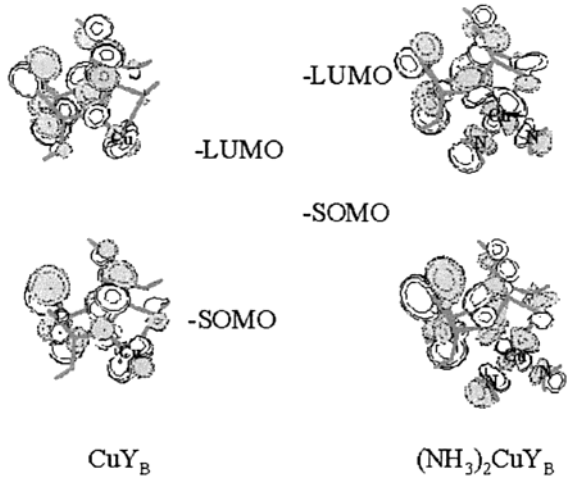

Figure 4. SOMO and LUMO contour plots of the CuY_B and $(H_3N)_2$-CuY_B.

2. Complexation with NH_3 of Cu(II)Z. We have shown that the choice of the model (size, Al distribution, cation position at site III) does not play a significant role in determining the electron distribution in the metal. Our next step is to verify that the choice of the model has also no effect with incoming reactants. To this purpose, we have analyzed how NH_3 binds to Cu in our different models and investigated the reactivity of CuY_B toward this ligand. The results obtained with NH_3 molecules are reported in Table 4, together with the complexes involving isolated Cu^{2+} and Cu^+ for comparison. In a recent work on gaseous complexes of Cu^{2+} with ammonia and water, it has been calculated that the tetracoordinated $Cu(NH_3)_4^{2+}$ is preferably almost square planar, with a C_{2v} symmetry.[42] A similar almost planar conformation has thus been adopted for ammonia complexes of CuY_B: first and second NH_3 molecules have been approached near to Cu, their nitrogen atoms lying in the plane defined by Cu and its two neighbors. The third NH_3 molecule in $(H_3N)_3CuY_B$ has been approached along the axis going through Cu and perpendicular to this plane. We have also verified that a tetrahedral conformation $(H_3N)_2CuY_B$ is less stable than the square planar structure.

Addition of two NH_3 on CuY_B does not change the frontier orbital profile characterized by a low lying empty orbital, but there is a change in their composition, as shown in Figure 4 (additional pN contribution to the orbitals). Addition of one ligand NH_3 to CuY_B and also to CuY_BH does not change the Cu−O bond lengths, whereas the addition of a second ligand leads to an increase (0.10 Å) of the shortest Cu−O distance.

The complexes of CuY_B and CuY_BH with one ammonia molecule have comparable geometries. Addition of a second ammonia yields two equivalent N−Cu bond lengths and the NH_3 geometries vary only by the HNH angles, which increase from 105.2 to 107.3−110.3°.

The general profile of the frontier orbitals remains the same when going from CuY_B and CuY_BH to H_3NCuY_B and H_3-$NCuY_BH$, i.e., keeping the characteristic small gap for Cu(II) and the large gap for Cu(I). It is interesting to analyze the evolution of the Cu electronic configuration when NH_3 molecules bind and to compare isolated and Cu zeolite cations (Table 4). NH_3 is a strong donor ligand: it donates already about 0.3 electron to Cu^+, accommodated in the 4s, 4p orbitals, the 3d subshell being already full. When one NH_3 molecule bonds to Cu^{2+}(isolated), its donation to Cu amounts to about 0.64 electron, which is essentially going into the empty 3d orbital. When four NH_3 molecules are bonded to Cu^{2+}, the total donation is around 1 electron (1.08) and the 4s, 4pσ, and 3dσ orbitals participate in the σ bonding molecular orbitals.

Comparing one NH_3 donation to isolated and Cu−zeolite ions shows that NH_3 transfers less charge to the cation when it is located in the zeolite: 0.13 to Cu(I) in CuY_BH instead of 0.27 to Cu^+ and 0.12 to Cu(II) in CuY_B instead of 0.64 to Cu^{2+}.

However, a more careful analysis describes the following result: each ammonia molecule always transfers around 0.2 electron to CuY_B and CuY_BH. But, in contrast with isolated cations, the ions involved in the zeolite do not systematically keep this charge.

Actually, in the case of one NH_3 bonded to CuY_B and one or two NH_3 bonded to CuY_BH, the CT to the zeolite models (about 0.2 electron in the three cases) is mostly distributed to the Cu-(II) and Cu(I) orbitals. However, further addition of NH_3 to CuY_B shows a reverse tendency with respect to the Cu net charge, which increases from +0.60 ($1NH_3$) to +0.74 ($2NH_3$) and +0.81 ($3NH_3$). In fact, the amount of charge transferred from the NH_3 ligands to CuY_B increases from 0.18 ($1NH_3$) to 0.38 ($2NH_3$) and 0.43($3NH_3$). The analysis of the NH_3 binding energies to CuY_B shows that the third ammonia is almost not bonded to the complex, which explains the small difference in the charge donation going from two to three ammonia ligands. Nevertheless, the interesting feature is that Cu does not retain the charge transferred from the additional NH_3 molecules, this charge being then distributed among the O atoms of the zeolite. Moreover, the Cu orbitals (essentially the 3d) are also transferring some electronic charge to the zeolite, increasing the hole in the 3d subshell. The presence of 2 or 3 NH_3 ligands have thus led to a modification of the electron distribution in the

zeolite-Cu entity, which behaves as a supermolecule. One can thus envisage that the zeolite can be a reservoir of charge that can be redistributed via the Cu cation.

Finally, the influence of the cluster size on the binding energy with NH_3 has been found negligible, on the basis of the results obtained for H_3NCuY_B and H_3NCuY_D. The addition of NH_3 to CuY_D has shown the same behavior as with CuY_B and with $jCuY_B$: the NH_3 binding energy is 43.7 kcal/mol for Cu in position P2 and 52.5 kcal/mol in position P3 (Figure 3).

Addition of NH_3 to $jCuY_B$ leads to a less stable structure $(H_3N)jCuY_B$ than $(H_3N)CuY_B$ and to a binding energy of 32.4 kcal/mol, whereas it is 49.9 kcal/mol for $(H_3N)CuY_B$. This large difference indicates that when Cu is bonded more strongly to the zeolite it is less available for additional interactions. Moreover, this result suggests that a Cu cation bearing molecular ligands can move along walls of the zeolite cavities in order to find more stable minima. The binding energies of ammonia to CuY_B and CuY_BH are compared in Table 4 with the binding energies of ammonia to isolated Cu(II) and Cu(I). It is obvious that the presence of the zeolite modifies the binding energies of NH_3 to Cu. As expected, CuY_B behaves similarly to CuY_BH, although NH_3 binding is slightly less for CuY_B than for CuY_BH. The binding energies of the ligands are strongly decreased in CuY_B with respect to isolated Cu^{2+}, whereas the difference is much smaller between CuY_BH and Cu^+. The binding energy of NH_3 decreases with the number of ligands, leading to almost no binding for the third NH_3 molecule on CuY_B.

Finally, B3LYP calculations with two different basis sets for the ligands have been compared with BP results. With the same basis (6-31G(d)), the average binding energies of ammonia are slightly smaller with B3LYP than with nl-BP: 48.3 and 33 kcal/mol with B3LYP vs 51.0 and 33.6 kcal/mol with nl-BP for $(H_3N)CuY_B$ and $(H_3N)_2CuY_B$, respectively. However, the use of the more extended basis set 6-311+G(2d,2p) decreases the B3LYP binding energy of NH_3 to CuY_B by 6 kcal/mol, showing that this property is more sensitive to the basis set extension than to the functionals.

IV. Conclusion

Our cluster model approach of a Cu(II)-exchanged faujasite has shown that a relatively small model is suitable to describe the electronic properties of the catalytic copper site. Although of limited size, this model includes real atoms and mimics the experimental coordination conditions of the transition metal cation. This study has demonstrated that the total number of Al being fixed by the cation formal charge and the electronic properties of the metal site are not very sensitive to the size of the cluster and to the topology of the Al distribution.

Comparison of various models and methodologies has led to the conclusion that the zeolitic framework is able not only to transfer electronic charge to the transition metal but also to receive charge from external ligands, if necessary. The calculated net charge on Cu is close to +1 and corresponds to a $3d^{10}$ configuration. However, the frontier orbital scheme of the Cu(II) site differs from that of a Cu(I) site, with the presence of a low-lying virtual orbital delocalized on the whole system (Cu−zeolite). The participation of additional ligands such as NH_3 in the HOMO explains how the charge can be transferred from one part to another of the supermolecular complex formed by the zeolite-cation−ligand system. Comparison of the Cu−zeolite and isolated Cu models with ammonia has clarified the mechanism in which electron donation from NH_3 ligands induces a rearrangement in the electronic structure of Cu with a clear participation of the zeolite framework, which plays the role of a reservoir of electronic charge. We may expect that this role is an important aspect in the reduction mechanism of NO by NH_3 on a Cu(II)-exchanged faujasite. Further work to analyze this aspect is in progress.

Acknowledgment. These calculations were carried out on the IBM SP2 computer of the CINES in Montpellier (Centre Informatique National de l′Enseignement Supérieur) and on the NEC-SX5 of the IDRIS (Institut des Ressources en Informatique Scientifique) in Orsay (France).

References and Notes

(1) Byrne, Y. W., 1990, U.S. Patent 4,961,917.
(2) Byrne, Y. W.; Chen, Y. M.; Speronello, B. K. *Catal. Today* **1992**, *13*, 33.
(3) Descat, G.; Hamon, C., 1994, U.S. Patent 5,369,070.
(4) Kieger, S.; Delahay, G.; Coq, B. *Appl. Catal. B* **2000**, *25*, 1.
(5) Hass, K. C.; Schneider, W. F. *J. Phys. Chem.* **1996**, *100*, 9292.
(6) Ramprasad, R.; Hass, K. C.; Schneider, W. F.; Adams, J. B. *J. Phys. Chem. B* **1997**, *101*, 6903.
(7) Schneider, W. F.; Hass, K. C.; Ramprasad, R.; Adams, J. B. *J. Phys. Chem.* **1996**, *100*, 6032.
(8) Schneider, W. F.; Hass, K. C.; Ramprasad, R.; Adams, J. B. *J. Phys. Chem. B* **1997**, *101*, 4353.
(9) Schneider, W. F.; Hass, K. C.; Ramprasad, R.; Adams, J. B. *J. Phys. Chem. B* **1998**, *102*, 3692.
(10) Nachtigallova, D.; Nachtigall, P.; Sauer, J. *Phys. Chem. Chem. Phys.* **1999**, *1*, 2019.
(11) Brändle, M.; Sauer, J. *J. Am. Chem. Soc.* **1998**, *120*, 1556.
(12) Greetbanks, S. R.; Hillier, I. H.; Sherwood, P. *J. Comput. Chem.* **1997**, *18*, 562.
(13) Goursot, A.; Arbouznikov, A.; Vasyliev, V. *Density Functional Theory: a Bridge between Chemistry and Physics.* In Proceedings of a two-day International Symposium organized under the auspices of the FWO−Flanders Scientific Network; Geerlings, P., De Proft, F., Langenaeker, W., Eds.; VUB Press: Brussels, Belgium, 1999; p 155.
(14) Walker, N. R.; Firth, S.; Stace, A. J. *Chem. Phys. Lett.* **1998**, *292*, 125.
(15) Stace, J. A.; Walker, N. R.; Firth, S. J. *J. Am. Chem. Soc.* **1997**, *119*, 10239.
(16) Hass, K. C.; Schneider, W. F. *J. Phys. Chem.* **1996**, *100*, 9292.
(17) Maxwell, I. E.; de Boer, J. J. *J. Phys. Chem.* **1975**, *79*, 1874.
(18) Kieger, S.; Delahay, G.; Coq, B.; Neveu, B. *J. Catal.* **1999**, *183*, 267.
(19) Olson, D. H. *Zeolites* **1995**, *15*, 439.
(20) Plévert, J.; Di Renzo, F.; Fajula, F.; Chiari, G. *J. Phys. Chem.* **1997**, *101*, 10340.
(21) Campana, L.; Selloni, A.; Weber, J.; Goursot, A. *J. Phys. Chem. B* **1997**, *101*, 9932.
(22) Casida, M. E.; Daul, C.; Goursot, A.; Koester, A.; Pettersson, L.; Proynov, E.; St-Amant, A.; Salahub, D. R.; Duarte, H.; Godbout, N.; Guan, J.; Jamorski, C.; Lebouf, M.; Malkin, V.; Malkina, O.; Sim, F.; Vela, A. deMon, *KS3*, University of Montreal, Montreal: 1996.
(23) Frisch, M. J.; Trucks, G. W.; Schlegel, H. B.; Scuseria, G. E.; Robb, M. A.; Cheeseman, J. R.; Zakrzewski, V. G.; Montgomery, J. A.; Stratmann, J. R. E.; Burant, J. C.; Dapprich, S.; Millam, J. M.; Daniels, A. D.; Kudin, K. N.; Strain, A. M. C.; Farkas, A. O.; Tomasi, J.; Barone, V.; Cossi, M.; Cammi, R.; Mennucci, B.; Pomelli, C.; Adamo, C.; Clifford, S.; Ochterski, J.; Petersson, G. A.; Ayala, P.; Cui, Y. Q.; Morokuma, K.; Malick, D. K.; Rabuck, A. D.; Raghavachari, K.; Foresman, J. B.; Cioslowski, J. J.; Ortiz, V.; Baboul, A. G.; Stefanov, B. B.; Liu, G.; Liashenko, A.; Piskorz, P.; Komaromi, I.; Gomperts, R.; Martin, R. L.; Fox, D.; Keith, J. T.; Al-Laham, M. A.; Peng, C. Y.; Nanayakkara, A.; Gonzalez, C.; Challacombe, M.; Gill, P. M. W.; Johnson, B.; Chen, W.; Wong, M. W.; Andres, J. L.; Gonzalez, C.; Head-Gordon, M.; Replogle, E. S.; Pople, J. A. Gaussian 98,*Gaussian 98, Revision A.7*, Gaussian, Inc.: *Pittsburgh*, PA, 1998.
(24) Vosko, S. H.; Wilk, L.; Nusair, M. *Can. J. Phys.* **1980**, *58*, 1200.
(25) Perdew, J. P.; Chevary, J. A.; Vosko, S. H.; Jackson, K. A.; Pederson, M. R.; Singh, D. J.; Fiolhais, C. *Phys. Rev. B* **1992**, *46*, 6671.
(26) Becke, A. D. *Phys. Rev. A* **1988**, *38*, 3098.
(27) Perdew, J. P. *Phys. Rev. B* **1986**, 33, 8822.
(28) Lee, C.; Yan, W.; Parr, R. G. *Phys. Rev.* **1988**, *B37*, 785.
(29) Becke, A. D. *J. Chem. Phys.* **1993**, *98*, 5648.
(30) Møller, C.; Plesset, M. S. *Phys. Rev.* **1934**, *46*, 618.
(31) Hoyau, S.; Ohanessian, G. *Chem. Phys. Lett.* **1997**, *280*, 266.
(32) Luna, A.; Amekraz, B.; Tortajada, J. *Chem. Phys. Lett.* **1997**, *266*, 31.
(33) Magnusson, E.; Moriarty, N. W. *Inorg. Chem.* **1996**, *35*, 5711.

(34) Thomas, J. L. C.; Bauschlicher, C. W. J.; Hall, M. B. *J. Phys. Chem. A* **1997**, *101*, 8350.
(35) Wachters, A. J. H. *J. Chem. Phys.* **1970**, *52*, 1033.
(36) Godbout, N.; Salahub, D. R.; Andzelm, J.; Wimmer, E. *Can. J. Chem.* **1992**, *70*, 560.
(37) Papaï, I.; Goursot, A.; Fajula, F.; Weber, J. *J. Phys. Chem.* **1994**, *98*, 4654.
(38) Bader, R. F. W. *Atoms in molecules. A quantum theory*; Clarendon Press: Oxford, 1990.
(39) Cotton, F. A.; Wilkinson, G. *Advanced Inorganic Chemistry*; John Wiley & Sons, Interscience Publishers: New York, London, Sydney, Toronto, 1972.
(40) El-Nahas, A. M.; Hirao, K. *J. Phys. Chem. A* **2000**, *104*, 138.
(41) Berthomieu, D.; Goursot, A.; Delahay, G.; Coq, B.; Martinez, A. Proceeding, 13th Internatinal Zeolite Conference, 2001, Montpellier (France), submitted.
(42) Bérces, A.; Nukada, T.; Margl, P.; Ziegler, T. *J. Phys. Chem. A* **1999**, *103*, 9693.